

## EXPERIMENTAL STUDY OF LATENT HEAT THERMAL STORAGE SYSTEM

### USING MIXED NANO PARTICLES WITH PCM

B.Prasanth<sup>1</sup>, S.Senthil kumar<sup>2</sup>, R.Baskar<sup>3</sup>, M.Ganesh Karthikeyan<sup>4</sup>.

<sup>1</sup>P.G Student, Department of Mechanical Engineering TRP Engineering College, Trichy

<sup>2,3,4</sup> Assistant professor, Department of Mechanical Engineering TRP Engineering College, Trichy

#### **Abstract:**

Thermal energy storage systems are necessary because the available energy like solar is intermittent whereas the utilization of thermal energy is continuous. The various methods of storing thermal energy are sensible heat storage, latent heat storage and thermo chemical storage, among this methods latent heat storage is preferred. Various materials are available to store thermal energy as latent heat; Paraffin is widely used phase change material (PCM). This is because paraffin maintains its properties even after thousands of charging and discharging cycles. This only disadvantage with paraffin is that its poor thermal conductivity. Increasing the metal nanoparticles composition in the paraffin increasing the thermal conductivity of the system, however there is a limit for blending the metal Nano particles with the PCM also. This is because; higher the metal Nano particle composition, higher will be the chance of agglomeration, which in turn decrease the thermal conductivity of the composite material. The performance characteristics of the thermal energy storage system are (i) Thermal conductivity of the PCM, (ii) Charging period and (iii) discharging period of thermal energy storage system. In this work, it is proposed to determine the suitable proportion of metal Nano particles that can be blended with paraffin PCM and analysis the performance of thermal energy storage system selected.

**Key word:** Phase change material, metal Nanoparticle, paraffin, latent heat storage

#### **1. Introduction**

Due to the extraordinary properties from their bulk form, nanoparticles have attracted considerable interest of research and applications [1,2]. In recent years, various sorts of nanoparticles can be produced because of the rapid advance in nanotechnology [3,4], greatly promoting the innovation in engineering and industrial processes [5]. For example, nanoparticles are used in thermal management to enhance the thermal conductivity of matrix materials [6,7]. The high conductivity of metal and/or metal oxide nanoparticles is used to improve the heat transfer of generally low conductivity fluids in mini- and micro-scale heat exchangers, such as in electronic devices and high capacity military communication devices [8,9].

Recently, He et al. [10] prepared water-based Zn nanofluids and measured their thermal conductivities. Results showed that the thermal conductivity of the nanofluid increased to a level greater than the prediction by the Hamilton-Crosser model [11,12]. Murshed et al. [13] measured the thermal conductivity of different nanofluids such as Zn /water, Zn/ethylene glycol, TiO<sub>2</sub> /water and TiO<sub>2</sub>/ethylene glycol; and found that the nanofluids had a higher thermal conductivity than respective base fluids. Xie et al. [14] revealed that the thermal conductivity of Zn nanofluid was higher than that of the base fluid and increased with increasing nanoparticles concentration level. The enhanced thermal conductivity ratio decreases with increasing pH value from 2.0 to 11.5. They also found that the

thermal conductivity of nanofluid varied with particle size and the optimal particle size for thermal conductivity enhancement was 60 nm.

Due to thermal energy storage can be used to enhance energy efficiency and to improve energy conservation and management, studies on thermal energy storage materials have attracted increasing attention in recent years [15,16]. Such materials can be categorized into sensible heat storage materials [17], latent heat storage materials [18], and thermal chemical materials. Latent heat storage uses phase-change materials (PCMs) that have much higher heat storage density and extremely smaller temperature variation during a phase-change process, compared with sensible heat storage materials. In comparison with thermal chemical materials and inorganic PCMs, organic PCMs have a proper phase-change temperature range, little or no super cooling, lower vapor pressure, no toxicity, non corrosives, and excellent thermal stability. Therefore, organic PCMs are one of the most preferred forms for thermal energy storage and have promising applications [18,19] in the field of solar energy storage, industrial waste energy storage, etc.

Fatty acids and paraffin wax (PW) are good organic PCMs due to their desirable characteristics such as high latent heat of fusion, negligible super cooling, low vapor pressure in the melt, and thermal stability [20]. However, the low thermal conductivity of fatty acids and n-alkanes is a major drawback, decreasing the rates of heat storage and retrieval during melting and crystallization processes, which in turn limit their utility capabilities.

Due to the improved thermal properties, materials with metal or metal oxide particles were commonly used to enhance heat transfer in energy conversion and management systems [21]. Therefore, studies have been carried out to develop latent heat thermal energy storage systems with enhanced thermal performance, like dispersing high conductivity particles and inserting a metal matrix into fatty acids [16,22]. In spite of the increased thermal conductivity, the relatively "big" particles in the organic matrix can be easily separated out from the composite [21]. However, nanoparticles in low concentration could remain separately in the composites because of their "Brown" motion in liquid. Recent advances of nanotechnology make it possible to exploit the development of stable organic phase-change composites.

In this study, Zn metal nanoparticles are carefully characterized by various analytical methods. The nanoparticles are then applied into a PW matrix to make phase-change composites. The thermal properties of the composites including melting point, latent heat capacity, and thermal conductivity at both solid and liquid states are investigated in detail.

## 2. Experimental Description

### 2.1. Characterization

Various methods have been applied to characterize the Al&Zn nanoparticle and Zn/PW composite samples. We used drynanoparticle samples without any other treatment. The scanning electron microscopy (SEM) observation was performed on a Hitachi S-4800 field emission SEM device. A polarizing optical microscope (POM) was also utilized to investigate the microstructure of the composites and the composite sample was put on a piece of silicon. The transmission electron microscopy (TEM) pictures were taken on a JEOL 2100F high resolution TEM device, in which the sample was scattered onto a copper mesh and observed directly under the instrument. Fourier transformation infrared (FTIR) spectra were measured in a range from  $4000\text{ cm}^{-1}$  to  $400\text{ cm}^{-1}$  via a Bomem DA8 spectrometer. In order to perform this analysis, 1mg sample was mixed with about 200 mg KBr crystal in a container and pressed into a tablet by a press tool. The x-ray diffraction (XRD) patterns were recorded on a D8-Advance

diffractometer using CuK $\alpha$  X-ray at 40 kV and 100 mA. The sample was put into a solid sample box and set onto the slot of the machine. The  $2\theta$  of XRD was scanned from  $10^{\circ}$  to  $90^{\circ}$ .

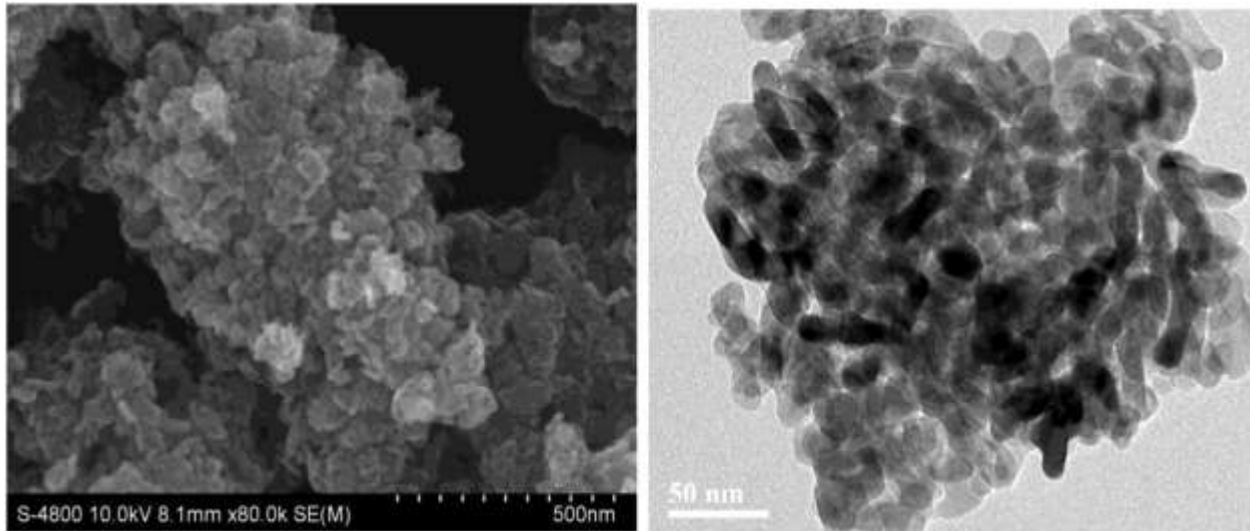


Figure 1. SEM (left) and TEM (right) images of our Zn Nanoparticles

## 2.2. DSC analysis

The thermal properties including the melting temperature and latent heat capacity of both the virgin PW and Zn/PW composites were measured using a differential scanning calorimetric (DSC) instrument. Indium was used as a reference during temperature calibration. Sample with mass of 3.00 ~ 5.00 mg was placed and pressed into a crucible at room temperature. A lid was placed on the sample to ensure an excellent thermal contact between the sample and the crucible. Then the crucible containing the sample was put into the DSC instrument in shielding nitrogen gas flow of 20 ml/min. After the 1 min remaining at the initial temperature, the DSC measurements were performed at a linear heating rate of  $5^{\circ}\text{Cmin}^{-1}$  in a temperature range from  $15^{\circ}\text{C}$  to  $65^{\circ}\text{C}$ . The temperature was maintained at  $65^{\circ}\text{C}$  for 1 min to remove thermal history, and then cooled down naturally to  $15^{\circ}\text{C}$ .

## 2.3. Thermal conductivity measurement

The thermal conductivity,  $k$ , of the virgin PW and the Zn/PW composites was measured by a transient short hot-wire method, and determined by the following formula [23]:

$$\frac{\partial T}{\partial \ln t} = \frac{q}{4\pi k} \text{----- (1)}$$

And thus,

$$k = \frac{q}{\frac{4\pi\delta T}{8\ln r}} = \frac{q}{4\pi t\theta(t)} \text{----- (2)}$$

Where q, t and  $\theta(t)$  are the applied heating power per unit length, the heating time and the temperature rise of the hot-wire, respectively. Initially the platinum wire immersed in the sample was at equilibrium with the surroundings. The uncertainty of this measurement is estimated to be  $\pm 2.0\%$  and the detailed estimation was available in Ref. [24]. For the thermal conductivity measurements, PCM sample was melted and poured into a stainless steel cylinder container. A platinum wire of 70  $\mu\text{m}$  in diameter and thermocouple were immersed in the PCM to record and test the temperature of the PCM before a waterproof lid covered the container. The platinum wire served as both a heating unit (hotwire) and an electrical resistance thermometer. The container was put into a water bath with specified test temperature of 20°C. A multimeter was used to test the current and voltage signals of the hot wire. When the thermocouple in the PCM showed a temperature vibration less than 0.1°C for 10 min, the hotwire in the sample started to probe. The hot wire probe was subjected from time  $t = 0$  to a step change in the electrical current applied to the wire. Then the temperature was set to other test point, to repeat the above steps. For each the test temperature, three measurements were conducted and the average value was taken.

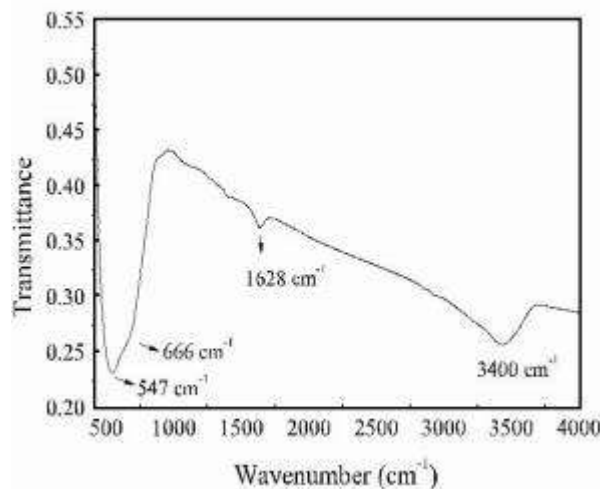


Fig.2 FTIR Spectrum of the Zn Particles

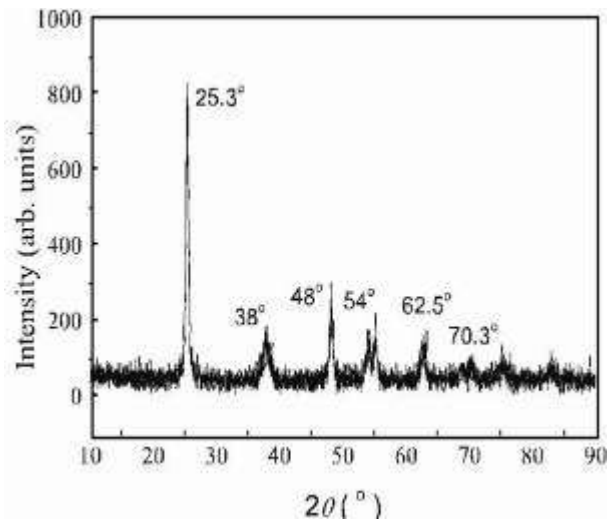


Fig.3 XRD Spectrum of the Zn Particles

## 2.4 Experimental Procedure for charging and discharging processes

The PCM based heat exchanger has to be incorporated with water heater. So, it is necessary to know the basic way of incorporating the thermal energy storage device with water heater. . Figure.4 shows the Schematic view of experimental setup.



**Fig.4**Experimental Setup

A storage tank is used to store the water which is having an electric water heater .Since we will be using a forced circulation, we need to incorporate a pump to maintain flow in the system. The water flow rate will be maintained by adjusting flow control valve. During the flow of hot water, the heat energy of the hot water is extracted by the paraffin wax available in the heat exchanger having helical coil made up of copper. By absorbing heat energy from hot water melting of paraffin wax will be occur. During the discharging, heat energy from paraffin wax will be absorbed by the water supplied through the heat exchanger. By adjusting the flow control valve, the flow rate of water will be changed .Here flow rate of water ranges from 0.01kg/min, 0.03kg/min and 0.06kg/min for both charging and discharging process of paraffin wax.

## 3. Results and discussion

### 3.1. Analysis of the Al&Zn particles

Fig. 1 shows the SEM and TEM images of the fabricated Al&Znparticles. Via observation, the averaged size of the nanoparticles is estimated smaller than 35 nm in diameter. The particles are columnar in shape. The nanoparticles clustered into groups because of the high surface energy with such small size.

Fig. 2 plots an FTIR spectrum of the Zn particles. The band at  $547\text{cm}^{-1}$  corresponds to the characteristic of band stretching vibration of Zn, which shifts to a longer wave number compared with the bulk Zn ( $540\text{cm}^{-1}$ ). The band transmitted at  $666\text{cm}^{-1}$  can be attributed to the characteristic of anatase form of Zn and it red shifts  $6\text{cm}^{-1}$  than the big crystal because of the incomplete crystal in the nanoscale size. The band at  $1628\text{cm}^{-1}$  and the broad band of  $3400\text{cm}^{-1}$  correspond to the characteristic of the O-H stretching of the water in the sample because the water combined in the sample couldn't be removed completely in the current synthesis conditions.

Fig. 3 is an XRD spectrum of the Zn particles. XRD is an important method to analyze the structure Of materials, especially for determining the phase of the crystalline. The spectrum clearly indicates that the particles are in the anatase form. Anatase characteristics are shown at  $25.3^{\circ}$  (101),  $38^{\circ}$  (004),  $48^{\circ}$  (200),  $54^{\circ}$  (105),  $62.5^{\circ}$  (204), and  $70.3^{\circ}$  (220). No impurity elements could be detected within the detection capability. The average diameter of the nanoparticles is about 25 nm calculated by the XRD data.

### 3.2. Compatibility of the composites

Fig.5 illustrates eight POM images of the composites in liquid (A to D) and solid (a to d) states, respectively. The particles were invisible in the images of the composite with 1.0 wt% Zn particles in both the liquid and solid states. For the composite with 3.0 wt% Zn particles, the presence of small particles is visible. When the loading is increased to 5.0 wt%, it is clearly seen that the Zn particles form into groups. The Zn groups tend to be in contact with neighboring groups when Zn loading is 7.0 wt%. In a liquid state composite of low concentration, solvation, "Brown" motion and electrostatic repulsion cause the nanoparticles separate individually. Probability of collision between nanoparticles increases with increasing concentration and Vander Waals force is stronger at a short range. Therefore nanoparticles tend to form groups in high concentration. The microstructure of the composite is different between the solid state and the liquid state, because PW molecules in solid state could push Zn into groups.

### 3.3. DSC analysis of the composites

It is of paramount importance to investigate the phase-change temperature and latent heat capacity of PCM. The molecules of PW will rotate and rearrange when they absorb heat at a certain temperature in the solid state. The transition of the microstructure of PW from a compact solid state

into a loose one indicates the occurrence of solid-solid phase change. When the temperature is further raised up to the melting point, the molecules of PW will absorb latent heat and convert into kinetic energy to overcome the intermolecular forces and turn the PW into the liquid state. In this work, DSC analysis was conducted to investigate the influences of the addition of Zn particles on the phase-change temperature and the latent heat storage capacity of the Zn/PW composites.

Fig.6 displays the DSC thermo grams of the Zn/PW composites with different particle concentration levels. The peaks on a DSC curve represent the phase-change behavior of a PCM. As shown on the figure, the Zn/PW composites have almost the same curve shape with the virgin PW.

Figs. 7 and 8 show how the phase-change temperature and the latent heat capacity of the composites vary with the loading of Zn particles, respectively. In Fig. 7,  $T_{s-s}$  and  $T_m$  represent the solid-solid phase-change temperature and solid-liquid phase-change temperature, respectively. Here the phase-change temperature is taken as the onset temperature of phase change at the DSC curves. The onset point is obtained as the temperature of intersection point between the tangent of the DSC curve at half height of the peak and the baseline. Therefore, the onset temperature is lower than the peak temperature at the DSC curve. It is seen that the phase change temperatures of the composite drop with loading at the beginning, but will come back with loading over 1 wt% for the  $T_m$ , and even increase for the  $T_{s-s}$ .

In Fig. 8,  $L_{s-s}$ ,  $L_{s-l}$  and  $L_{total}$  represent the latent heat capacities of the solid-solid phase change, solid-liquid phase change, and their sum, respectively. Interestingly, both  $L_{s-s}$  and  $L_{s-l}$  of the composites have the highest value when the Zn particle loading is at 0.7 wt%. For example, the  $L_{s-l}$  for the composite with 0.7 wt% is greater than that of virgin PW by 20.1 J/g. When the loading is over 2 wt%, the latent heat capacities are actually lower than those of the virgin PW. In general, there are at least two opposite factors that cause the latent capacity change in the composite: 1) the interaction between the Al and Zn particles will increase the latent capacity of the composites; and 2) the addition of the Zn particles would reduce the latent heat capacity because the replacement of nanoparticles for the PW molecules could lead to absorb or release more energy during composite melting or solidification processes. So the latent heat capacity of the composite would increase if the first factor were stronger than the second one and vice versa. As shown in Fig. 5, Zn particles grow into groups and the groups getting bigger with increasing particle loading. This microstructure of the composite showed that the Al particles could push Zn particles during phase change processes and this explains the trend showing in Figs. 7 and 8.

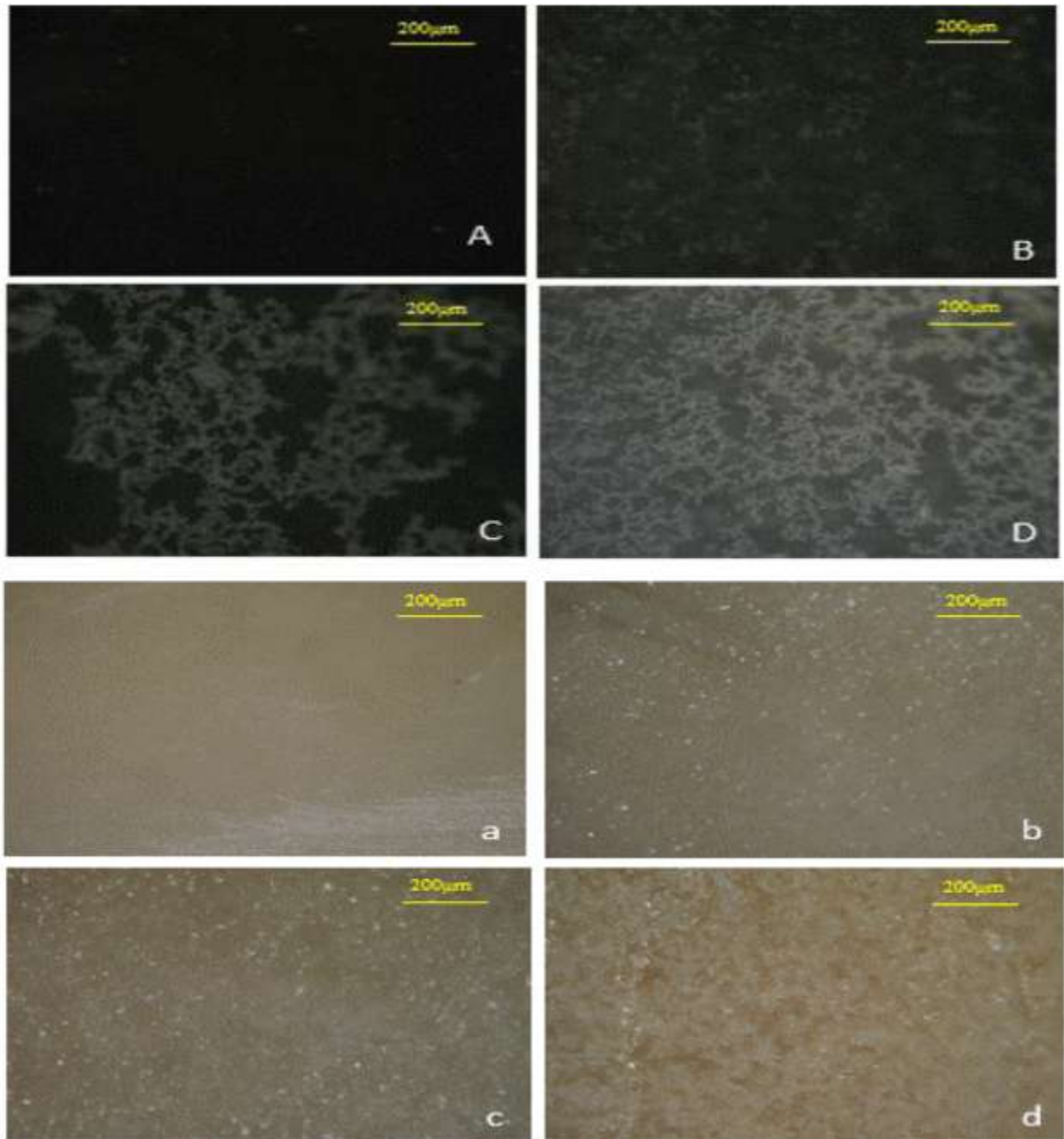


**Fig.5** POM images of Al&Zn composites with 1.0 wt% (A),3.0wt% (B),5.0 Wt% (C),7.0 wt% (D) in solid state



### 3.4. Thermal conductivity of the composites

The rate of energy storage or release is highly dependent on the thermal conductivity of material. Al&ZnPCMs have high potentials to be used as efficient thermal energy storage materials at environmental temperature range. We measured the thermal conductivity of the composites at different temperatures to show how the thermal conductivity changes with temperature and phase state. The major test temperatures are 20, 40 and 60°C, respectively. At 20°C, the composites are in the solid state prior to solid-solid phase change. At 40°C, they are before solid-liquid phase change, but have experienced solid-solid phase change. At 60°C, the composites are in the liquid state completely. So these three temperature points present three phases of the PCMs studied.

Theoretically, the thermal conductivity of composites can be estimated as follows [25]:

$$k_c = \phi_v \times k_p + (1 - \phi_v) \times k_f \text{----- (3)}$$

Where  $\phi_v$  is the particle volume fraction in the composite; and  $k_c$ ,  $k_p$  and  $k_f$  are thermal conductivities of the composite, the nanoparticle and the matrix, respectively. The relationship between volume fraction and weight fraction  $\phi_w$

$$\phi_v = \phi_w \times \left( \frac{\rho_c}{\rho_p} \right) \text{----- (4)}$$

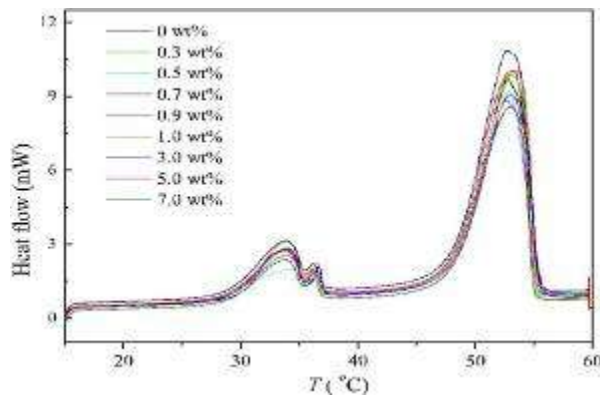


Fig.6 DSC curves of the composites

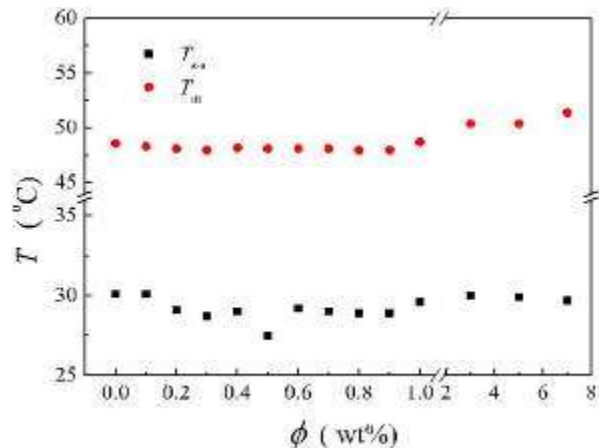


Fig.7 Phase change temperatures of PW and Zn/PW composites

Fig. 9 depicts the dependence of the thermal conductivity of the Zn/PW composites on the Zn loadings in the three test temperatures. The discrete symbols in the figure represent experimental measurements and the dotted lines are from theoretical predictions. For the three test temperatures, it is seen that  $k$  decreases with increasing temperature; but increases with increasing loading of the Zn nanoparticles. However, the measured enhancement of the thermal conductivity is lower than the theoretical prediction, in particular at higher loadings over 3 wt%. There are many factors that affecting the stability of liquid composite, including attractive and repulsive forces among particles, and “Brown” motion. The “Brown” motion and repulsive force between particles would keep the particles separate in the composite, while the attractive forces cause a tendency in liquids to resist separation. The repulsive forces are

stronger than the attractive forces in liquid composites with lower concentration, and vice versa with higher concentration. Therefore, nanoparticles in higher concentration composites are easily aggregated, as seen in Fig. 5.

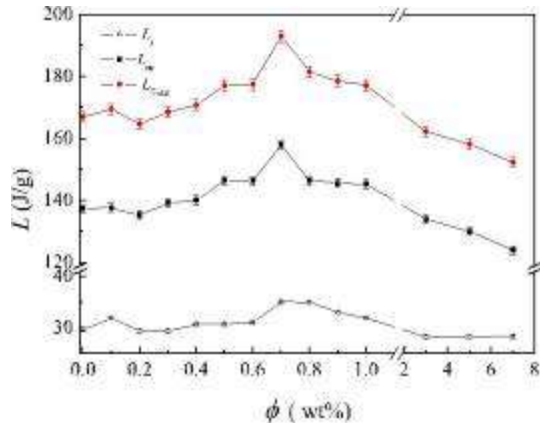


Fig.8 Latent heat capacity of PW and Zn composites

Grouping of nanoparticles increases thermal resistance; and therefore, aggregation decreases the thermal conductivity of composite. This could partially explain why the experimental measurement is lower than the theoretical prediction. Interfacial thermal resistance between the nanoparticles and the matrix molecules was accounted as a dominant fact for the discrepancy [24].

represents the thermal conductivity of the virgin PW. It is seen that the thermal conductivity is enhanced with increasing load of Zn nanoparticles, except for cases at 60°C with 1.0wt%, at 40°C with 0.7 and 5.0 wt% loading. As seen in Fig. 5, particles in 1.0 wt% Zn/PW begin turning into groups in the liquid state. Grouping consumed free particles which enhance thermal conductivity in composite. Therefore, the thermal conductivity at 60°C with 1.0 wt% is lower because it is in the liquid state. From Fig. 6 we can see that the composite solid-solid phase changed when temperature arose to 40°C. During the phase change, PW molecules could push the particles to form groups. This might be the reason for the thermal conductivity of 0.7 wt% Zn/PW lower than that of 0.5 wt% Zn/PW. When the concentration is increased to 5.0 wt%, the particle groups become very big and the number of groups decreases as shown in Fig. 5(C). This may be the reason of lower thermal conductivity in 5.0 wt% Zn/PW at 40°C.

Fig. 10 shows the thermal conductivity

enhancement percentages subjected to different Zn loading levels at the three test temperatures. In the figure,  $k_0$

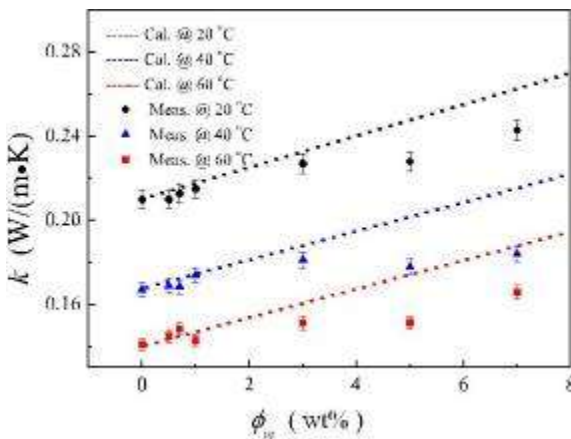


Fig.9 Thermal conductivity Vs Zn mass loading

Fig. 11 shows the dependence of thermal conductivity of the composites on temperature for different loadings. The temperature ranges from 15 °C to 65°C. It is seen that the thermal conductivity of the composites decreases with increasing temperature and phase change. The structure of composite relaxed whenever it experienced a phase change. This is why the thermal conductivity at the solid state (15-25°C) is greater than its counterpart at another solid state at 35°C and 40°C; and the value is the lowest at the liquid state (55-65°C).

### 3.5 Charging process of PWZncomposites

The charging process was carried by applying heat transfer fluid (HTF) with a flow rate of 0.01kg/min, The HTF is flowing through the storage tank then the temperature of raw paraffin and PW/ Zncomposites at various proportion of Zn nano particles have been noted for every 10 minutes once. The temperature profiles for pcm and PW/ Zncomposites have been drawn for each level as shown in fig.12. This procedure was carried for HTF flow rate of 0.03kg/min and 0.06kg/min and the corresponding temperature profiles for pcm and PW/ Zncomposites have been drawn for each level as shown in fig.13 and fig.14.

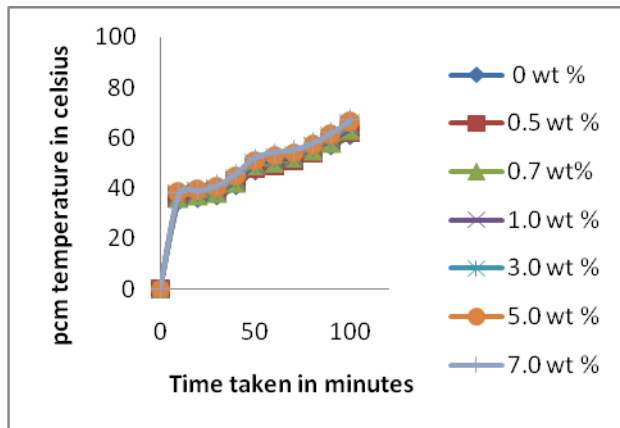


Fig.10 Temperature profile of pcm for

$$\dot{m} = 0.01 \text{ kg/min}$$

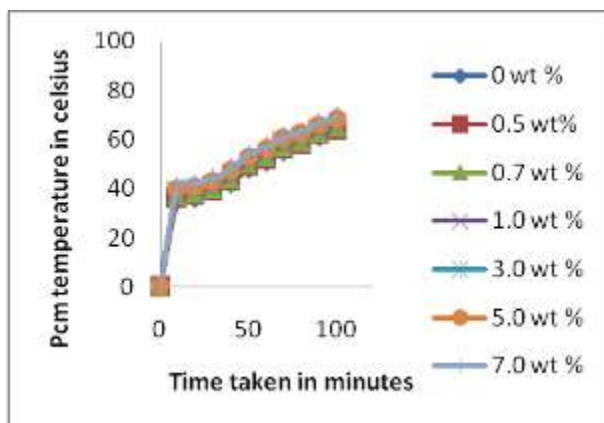


Fig.11 Temperature profile of pcm for

$$\dot{m} = 0.03 \text{ kg/min}$$

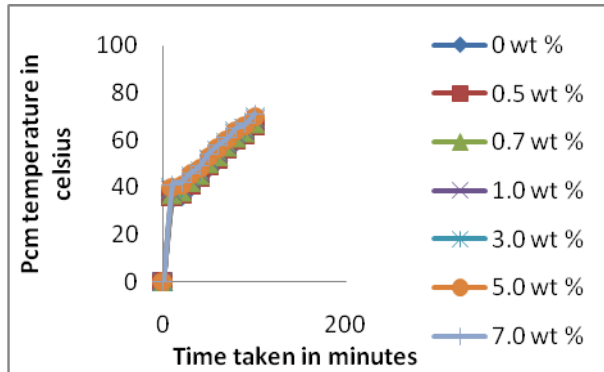


Fig.12 Temperature profile of pcm for

$$\dot{m} = 0.06 \text{ kg/min}$$

From fig.12, fig.13 and fig.14, it is clear that the temperature of pcm is increasing with the increase in mass loading of Zn nano particles and hence charging Period of PW/ Zn composites is reduced.

### 3.6 Discharging process of PW Zncomposites

The discharging process was carried by applying water at room temperature with a flow rate of 0.01kg/min, The water is flowing through the storage tank then the temperature of raw paraffin and PW/ Zn composites at various proportion of Zn nano particles have been noted for every 10 minutes once. The temperature profiles for pcm and PW/ Zn composites have been drawn for each level as shown in fig.15 This procedure was carried for HTF flow rate of 0.03kg/min and 0.06kg/min and the corresponding temperature profiles for pcm and PW/ Zn composites have been drawn for each level as shown in fig.16 and fig.17.

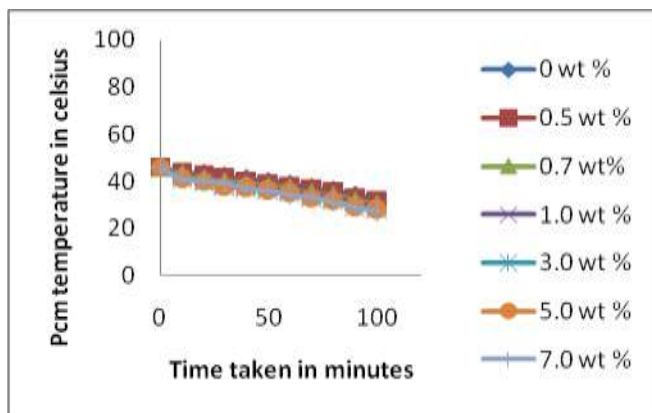


Fig.13 Temperature profile of pcm for  $\dot{m} = 0.01 \text{ kg/min}$

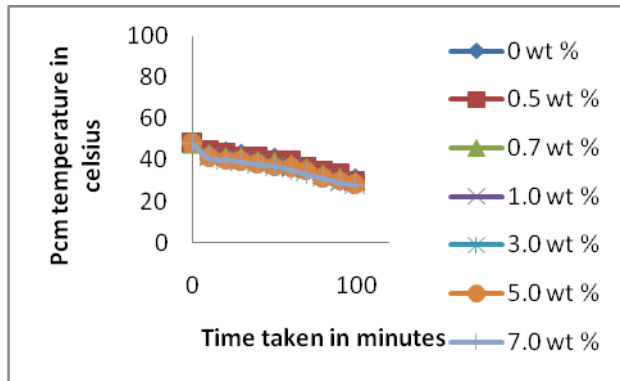


Fig.14 Temperature profile of pcm for  $\dot{m} = 0.03\text{kg}/\text{min}$

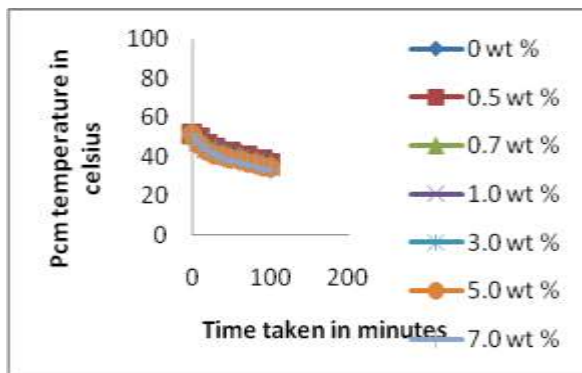


Fig.15 Temperature profile of pcm for

$\dot{m} = 0.06\text{kg}/\text{min}$

From fig.15, fig.16 and fig.17, it is clear that the temperature of pcm is decreasing with the increase in mass loading of Zn nano particles and hence discharging Period of PW/ Zn composites is reduced.

#### 4. CONCLUSIONS

The Al&Znnanoparticles analyzed the particle size and properties by various analytical methods including the SEM, TEM, FTIR and XRD. Results showed the Al&Znnanoparticles in the anatase form and about 30 nm in size. The Al&Znnanoparticles were added into melted PW to make Al&Zn composites. The addition of Znnanoparticles will reduce the phase change temperatures with low loading levels, but increase the solid-liquid phase-change temperature when the loading is over 1 wt%. The latent heat capacity will increase when the loading level is below 1.0wt%, with maximum value around 0.7 wt%. Further increasing the loading will actually reduce the

latent heat capacity. The thermal conductivity of Al&Zn composites increases with increasing Zn nanoparticles loading, and decreases with increasing temperature. The thermal conductivity of the composites is lower in the liquid state than in the solid state. The charging and discharging time are reduced by increasing the mass loading of Al&Zn nano particles.

## 5. REFERENCES

- [1] G. Cao, Annual Review of Nano Research, World Scientific, Singapore, New Jersey, 2006.
- [2] J. Reineke, Nanotoxicity: Methods and Protocols, Humana Press, New York, 2012.
- [3] T. Amna, M.S. Hassan, K.T. Nam, Y.Y. Bing, N.A.M. Barakat, M.S. Khil, H.Y. Kim, Preparation, characterization, and cytotoxicity of CPT/Fe<sub>2</sub>O<sub>3</sub>-embedded PLGA ultrafine composite fibers: a synergistic approach to develop promising anticancer material, *Int. J. Nanomed.* 7 (2012) 1659-1670.
- [4] Y.H. Cheng, Y.F. Kang, L.W. Wang, Y. Wang, S.R. Wang, Y.J. Li, W. Zhong, L.Q. Peng, Preparation of porous alpha-Fe<sub>2</sub>O<sub>3</sub>-supported Pt and its sensing performance to volatile organic compounds, *J. Nat. Gas Chem.* 21 (2012) 11-16.
- [5] X.Q. Zha, J.J. Xiao, H.N. Zhang, J.H. Wang, L.H. Pan, X.F. Yang, J.P. Luo, Polysaccharides in *Laminaria Japonica* (LP): extraction, physicochemical properties and their hypolipidemic activities in diet-induced mouse model of atherosclerosis, *Food Chem.* 134 (2012) 244-252.
- [6] L. Colla, L. Fedele, M. Scattolini, S. Bobbo, Water-based Fe<sub>2</sub>O<sub>3</sub> nanofluid characterization: Thermal conductivity and viscosity measurements and correlation, *Adv. Mech. Eng.* 2012 (2012) 1-8.
- [7] E. Bahar, N. Ucar, A. Onen, Y.J. Wang, M. Oksuz, O. Ayaz, M. Ucar, A. Demir, Thermal and mechanical properties of polypropylene nanocomposite materials reinforced with cellulose nano whiskers, *J. Appl. Polym. Sci.* 125 (2012) 2882-2889.
- [8] R. Kandasamy, X.Q. Wang, A.S. Mujumdar, Application of phase change materials in thermal management of electronics, *Appl. Therm. Eng.* 27 (2007) 2822-2832.
- [9] F.L. Tan, C.P. Tso, Cooling of mobile electronic devices using phase change materials, *Appl. Therm. Eng.* 24 (2004) 159-169.
- [10] Y. He, Y. Jin, H. Chen, Y. Ding, D. Cang, H. Lu, Heat transfer and flow behavior of aqueous suspensions of TiO<sub>2</sub> nanoparticles (nanofluids) flowing upward through a vertical pipe, *Int. J. Heat Mass Transfer* 50 (2007) 2272-2281.
- [11] R.L. Hamilton, O.K. Crosser, Thermal conductivity of heterogeneous two component systems, *Ind. Eng. Chem. Fundam.* 1 (1962) 187-191.
- [12] W. Yu, S.U.S. Choi, The role of interfacial layers in the enhanced thermal conductivity of nanofluids: a renovated Hamilton-Crosser model, *J. Nanopart. Res.* 6 (2004) 355-361.
- [13] S.M.S. Murshed, K.C. Leong, C. Yang, Investigations of thermal conductivity and viscosity of nanofluids, *Int. J. Therm. Sci.* 47 (2008) 560-568.
- [14] Thermal Conductivity of Wurtzite Zinc-Oxide from First-Principles Lattice Dynamics – a Comparative Study with Gallium Nitride Xufei Wu, Jonghoon Lee, Vikas Varshney, Jennifer L. Wohlwend, Ajit K. Roy & Tengfei Luo (March 2016)-22504.
- [15] D.W. Yoo, Y.K. Joshi, Energy efficient thermal management of electronic components using solid-liquid phase change materials, *IEEE Trans. Device Mater. Reliab.* 4 (2004) 641-649.
- [16] B. Zalba, J.M. Marin, L.F. Cabeza, H. Mehling, Review on thermal energy storage with phase change materials, heat transfer analysis and applications, *Appl. Therm. Eng.* 23 (2003) 251-283.
- [17] F. Abniki, E. Bakhshi, M. Mosalla. The sensible heat storage by phase change materials, *Petroleum Preprints Presented at the 235th ACS National Meeting, New Orleans, 6-10 April 2008*, p. 110.

- [18] F. Agyenim, N. Hewitt, P. Eames, M. Smyth, A review of materials, heat transfer and phase change problem formulation for latent heat thermal energy storage systems (LHTESS), *Renewable Sustainable Energy Rev.* 14 (2010) 615-628.
- [19] E.M. Alawadhi, Using phase change materials in window shutter to reduce the solar heat gain, *Energ. Buildings* 47 (2012) 421-429.
- [20] P.E. Arndt, J.G. Dunn, R.L.S. Willix, Organic-compounds as candidate phase change materials in thermal-energy storage, *Thermochim. Acta* 79 (1984) 55-68.
- [21] J.A. Khan, X. Tong, M.R. Amin, Enhancement of heat transfer by inserting a metal matrix into a phase change material, *Numer. Heat Transfer Part A* 30 (1996) 129-131.
- [22] J. Wang, H. Xie, Z. Xin, Y. Li, Y. Chou, Investigation on thermal properties of heat storage composites containing carbon fibers, *J. Appl. Phys.* 110 (2011) 094302.
- [23] P. Bhattacharya, S. Saha, A. Yadav, P. Phelan, R. Prasher, Brownian dynamics simulation to determine the effective Thermal conductivity of nanofluids, *J. Appl. Phys.* 95 (2004) 6492.
- [24] H.Q. Xie, T.G. Xi, J.C. Wang, Study on the mechanism of heat conduction in nanofluid medium, *Acta Phys. Sin.* 52 (2003) 1444-1449.